# Simulation of a malaria nanoplasmonic biosensor based on extraordinary optical transmission

**A. S. Kiyumbi and M. S. Tame**

Department of Physics, Stellenbosch University, Private Bag X1, Matieland 7602, South Africa

E-mail: akiyumbi@gmail.com

**Abstract.** In this study, we present the theoretical analysis and optimization of a 2D metasurface made from gold for sensing Plasmodium falciparum (Pf) parasites. The sensor is made of equal distance periodic circular nanoholes on a gold planar surface. Specifically, it is an array of nanoholes patterned in a 100 nm thick gold film where the diameter of nanoholes is 150 nm and the center-to-center separation is 400 nm. When probed by light, these nanoholes give rise to extraordinary optical transmission resonant peaks resulting from the hybridization between surface plasmons and optical modes inside nanoholes. By monitoring the shift of transmission peaks or transmission intensity, the induced refractive index perturbation due to Pf-antibody-antigen interactions can be accurately measured. We report a minimum limit of detection of $3.19\times 10^{-4}$ RIU using spectral interrogation and $1.00\times 10^{-4}$ RIU using intensity interrogation. These sensor properties can be useful for the diagnosis of malaria at an early stage.

## 1. Introduction

Malaria, a mosquito-borne disease has infected humans for centuries. In 2020, malaria resulted in 627,000 deaths globally. Africa made up 96% of global malaria deaths and about 80% of all deaths in the region were children under 5 years [1]. Conventional malaria diagnosis is based on empirical therapy, antibody rapid diagnostic tests (mRDTs), nucleic acid-based molecular analysis, and/or microscopic analysis [2]. These methods are limited in precision, affordability, integration, or portability. They also require long detection times, sophisticated infrastructure, and trained personnel [3]. For example, mRDTs have various well-known detection problems [4]. To overcome these diagnosis limitations, researchers are interested in designing different kinds of optical biosensors to in-vitro detect malaria parasites [5]. For example, 1D and 2D photonic crystal biosensors and surface plasmon resonance biosensors for malaria detection [8, 9, 10]. Recent progress in the development of malaria diagnostic tests, potential biomarkers, and their applications are summarised in reviews by Ragavan et al. [5] and Priyamvada et al. [11].

In this work, we design, simulate, and analyze a malaria plasmonic biosensor based on extraordinary optical transmission (EOT) that operates in the visible and near infra-red optical regime ($\lambda$= 450 nm to 850 nm). The biosensor is made up of a metasurface with periodic nanoholes 150 nm in diameter and 400 nm apart patterned in a gold film (100 nm thick) and deposited onto a glass substrate. The finite element numerical method, using COMSOL Multiphysics has been utilized for modeling and simulation. The spectral sensitivity and limit of detection are calculated and their contribution to sensing is discussed.

## 2. Theoretical background

Surface plasmon resonance (SPR) biosensing is a practical and commercial label-free diagnostic technique that enables the investigation of ligand-receptor interactions by utilizing surface plasmon waves [12]. The technique offers real-time analysis and immediate recognition of biomolecular species and their interactions. Surface plasmons (SPs) are electromagnetic excitations propagating and evanescently confined at a metal-dielectric interface. They arise due to the coupling of an incident transverse electromagnetic wave to oscillations in the metal's electron plasma [13]. These surface modes are a self-consistent solution of the 3D Maxwell equations and are characterized in terms of their dispersion according to [13]

$$k_{sp} = k_0 \sqrt{\frac{\varepsilon_m \varepsilon_d}{\varepsilon_m + \varepsilon_d}}. \tag{1}$$

Here, $k_{sp}$ is the propagation constant of surface plasmons, $k_0 = \frac{2\pi}{\lambda}$ the propagation constant of an incident photon in free space, $\lambda$ is the excitation wavelength, and $\varepsilon_m$ and $\varepsilon_d$ are the permittivity of the metal and the adjacent dielectric. Due to momentum mismatch, $k_{sp} > k_0$, and so it is difficult to excite SPs by direct probing of the metal surface.

Periodic nanohole arrays structured on metals are a class of 2D photonic grating that allows the direct excitation of SPs. When a wave polarised along one of the array axes is incident on this structure, the array exhibits EOT. The phenomenon was first reported by Ebbesen [14]. The name EOT is used because the amount of transmitted light ($T$) through a sub-$\lambda$ hole (diameter $d \ll \lambda$) is much higher than what could be expected by Bethe's classical aperture theory [15]. The EOT phenomenon is the result of a hybridization between SPs, quasi-cylindrical waves, and optical modes inside nanoholes [16, 17, 18]. Plasmon properties of the film material ("metal transparency window") in the spectral range of measurement are also important to realize the EOT effect and hence EOT is sometimes related to the excitation of a Fabry–Perot resonance in holes. The physics and detailed explanation of EOT through periodic nanohole arrays in real metals have been examined in Refs. [19, 20]. Analytical derivations and models that provide deeper insight are also formulated to capture the essential mechanisms involved in this phenomenon [21]. At resonance, the wavelength of light that can be transmitted, $\lambda_{sp}$, through periodic nanoholes is given by

$$\lambda_{sp} = \frac{a_0}{\sqrt{i^2 + j^2}} \sqrt{\frac{\varepsilon_m \varepsilon_d}{\varepsilon_m + \varepsilon_d}}, \tag{2}$$

where $a_0$ is the lattice constant (i.e. distance between nanoholes), and $i$ and $j$ are non-zero integer numbers representing scattering orders of the surface wave.

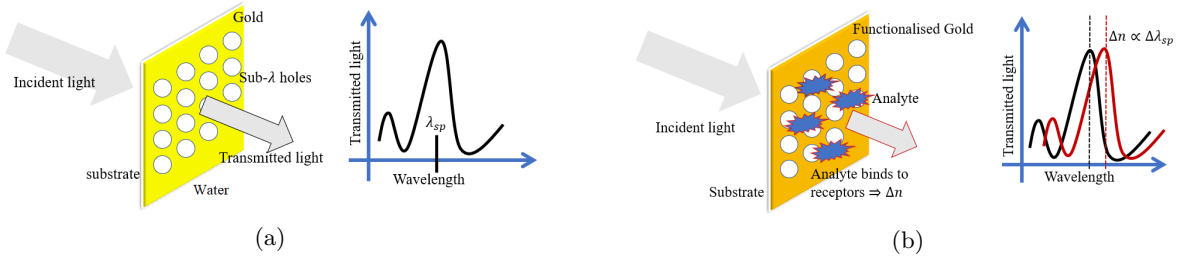


Figure 1: (a) A schematic drawing of the designed EOT-based SPR sensor showing the main three components of the sensor, the substrate layer (glass), nanohole array (optical transducer), and the analyte layer (e.g. water). (b) The working principle of the sensor. When the target analyte (in water or blood) binds to the receptors immobilized on the gold surface, the refractive index $n$ near the metal surface is altered. A change in $n$ results in a change of maximum transmission wavelength $\lambda_{sp}$. By monitoring this change, EOT-based sensing is attained.

From Eq. (2), the adsorption of ligand molecules to immobilized receptors in the vicinity of a metal-dielectric interface alters the dielectric refractive index $n = \sqrt{\varepsilon_d}$, which then alters the coupling condition and hence shifts the resonant wavelength $\lambda_{sp}$ of transmission maximum(s). The ligand molecules (or target analytes) are then detected based on the shift of $\lambda_{sp}$. However, EOT resonances are also tunable through the engineering of hole shape, hole size, and periodicity [22, 23], this adds another avenue for designing EOT-based sensors. Fig. 1(a) shows the designed EOT-based SPR sensor. The working principle of the sensor is summarised in Fig. 1(b).

## 3. Modeling and simulation

The finite element method was performed using COMSOL multiphysics to simulate the optical transmission response of the periodic nanohole array patterned on a gold film, as shown in Fig. 2(a). The model geometry is discretized into finite elements formed by 2D and/or 3D meshing. At points where these elements meet (nodes), a set of linear partial differential Maxwell equations are iteratively solved. Solutions of individual elements need to converge to obtain the whole model solution. Floquet periodic boundary conditions are usually used to address periodic nanoholes but due to the symmetry of the modeled geometry and to save computational time, a quarter of the unit cell is simulated. The two boundaries perpendicular to the x-axis and y-axis were set as perfect electric conductors (PEC) and perfect magnetic conductors (PMC), respectively. They work as absorbing layers for an incident p-polarised or s-polarised light propagating into unbounded space. The top and bottom domain of the sensor structure are declared as the analyte layer ($n_d = 1.33$ to $n_d = 1.38$) and the substrate layer (glass, $n_s = 1.52$), respectively. The middle domain is the gold film perforated with a subwavelength hole. The adhesion layer between glass and gold film and the analyte binding layer between gold and a bioreceptor are both ignored in this model because their inclusion only slightly affects the spectral locations of the resonances. The choice of $n_d$ for the analyte layer is practical in malaria diagnosis since the refractive index of blood cells in different stages of malaria lies in that range. Normal stage $n = 1.408$, ring stage $n = 1.396$, trophozoite stage $n = 1.381$ and schizont stage $n = 1.371$ [6, 24]. Variation of refractive index in blood cells is due to the change in the haemoglobin concentration in the blood sample from healthy to an infected one. However, these values are just baseline values. When the analyte binds to receptors, baseline values would change by a small amount $\delta n$, which is more important in biosensing as it corresponds to a specific binding process. The modified Lorentz-Drude model was used to include the frequency-dependent $\varepsilon_m$ of gold [25]. A normal TM-polarized plane wave incident from the substrate side is used as an optical excitation. To avoid undesired numerical reflections back into the interior of a computational region, the top and bottom boundaries of the model system are terminated by strong absorbing perfectly matched layers (PML).

## 4. Result and Discussion

To determine the sensitivity and the limit of detection, we modeled the expected experimental response of our sensor by imposing an experimental white light spectrum into the simulated spectra shown in Fig. 2(b). The spectrum of a white light LED source adds the necessary noise to our simulated spectra. This noise stems from the spectrometer and shot noise from the statistical nature of the light. We are interested in the total noise as this is what puts a lower bound on the limit of detection in a real experiment. The transmission spectra in Fig. 2(c) are the expected experimental results when a MBB1F1 fiber-coupled light emitting diode (LED) from Thorlabs is used to illuminate the sensor. Using a moving standard deviation algorithm, the fluctuation of intensity $\Delta I$, which represents noise in the sensor output was plotted against $\lambda$, see inset in Fig. 2(c). Our analysis focuses on the first and second peaks at around 650 nm and 740 nm respectively. The peak around 500 nm is ignored in sensing analysis because is an intrinsic property of the gold film associated with the interband transition.

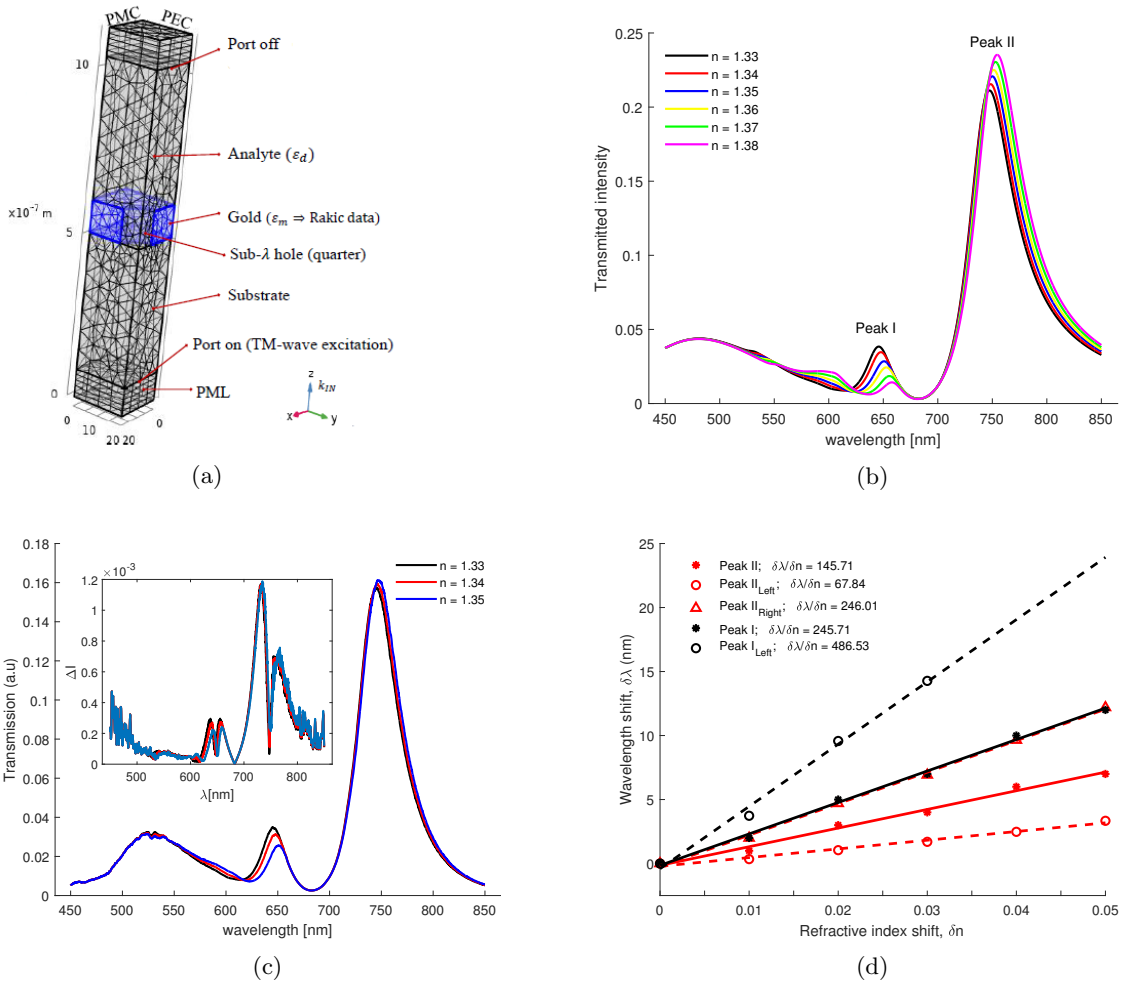


Figure 2: (a) A COMSOL model of the sensor system showing a quarter of the unit cell. PEC and PMC boundary conditions are applied perpendicular to the x and y-axes. (b) The simulated transmission spectra of the gold nanohole array in liquid analyte with a refractive index ranging from $n = 1.33$ to $n = 1.38$. (c) Modeled experimental transmission spectra of the sensor and the associated intensity fluctuation $\Delta I$ (inset figure) plotted against $\lambda$. Both the main figure and its inset share the same legend. (d) Spectral sensitivity $\delta\lambda/\delta n$ (where $\delta n = n - 1.33$) around peak I and peak II shows that the left of peak I is the most sensitive peak.

From Fig. 2(d), a small change in refractive index $\delta$n from a baseline of $n = 1.33$, linearly shifts the position of the transmission maxima by $\delta\lambda$. One can also fix the wavelength and monitor changes in the transmitted intensity $\delta I$ at that wavelength. Therefore, the sensitivity $S_{RI}$ of our sensor is defined as the extent to which the intensity or wavelength changes for a given change of the refractive index $\delta n$ when $\lambda$ or $I$ is fixed. The limit of detection (LOD), the minimum detectable change of the refractive index $\Delta n$, is linked to $S_{RI}$ by [26, 27]

$$\text{LOD} = \Delta n = \frac{\Delta Y}{S_{RI}}. \tag{3}$$

Here, $Y$ is an explicit observable parameter (intensity or wavelength) that changes with respect to $\delta n$, and $S_{RI} = \left|\frac{\delta Y}{\delta n}\right|$ at a fixed $\lambda$ or $I$ and $\Delta Y$ is the noise associated with the measurement of $Y$. Therefore, the practical functionality of the SPR sensor depends on the sensitivity $S_{RI}$ and the noise $\Delta Y$ in the sensor output which depends on the system parameters, $\lambda$ and $n$. The

inset of Fig. 2(c) shows a strong $\lambda$ dependence of $\Delta I$ and by changing $n$ we found a weak $n$ dependence of $\Delta I$. Furthermore, we found that the sensitivity $S_{RI}$ weakly depends on the baseline $n$ for intensity or wavelength sensing and that $\frac{dY}{dn} = \lim_{\delta n \to 0} \frac{\delta Y}{\delta n}$, we then have for intensity or wavelength sensing

$$\text{LOD} = \left|\frac{\delta n}{\delta I}\right|_\lambda \Delta I = \left|\frac{\delta I}{\delta n}\right|_\lambda^{-1} \Delta I, \tag{4}$$

or

$$\text{LOD} = \left|\frac{\delta n}{\delta \lambda}\right|_I \Delta\lambda = \left|\frac{\delta n}{\delta \lambda}\right|_I \left|\frac{\delta \lambda}{\delta I}\right|_I \Delta I = \left|\frac{\delta \lambda}{\delta n}\right|_I^{-1} \left|\frac{\delta I}{\delta \lambda}\right|_I^{-1} \Delta I. \tag{5}$$

In Fig. 3(a), we show a linear relation between $\delta I$ and $\delta n$ at a fixed $\lambda = 645$ nm and extract out the intensity sensitivity $S_{RI}^I = \left|\frac{\delta I}{\delta n}\right|_{\lambda=645\text{nm}} = 0.6366$ RIU$^{-1}$. Using this value in Eq. (4) together with the noise $\Delta I(\lambda)$ shown in the inset of Fig. 2(c), the LOD at 645 nm is calculated as $1.52 \times 10^{-4}$ RIU. The LOD data plotted against $\lambda$ shown in Fig. 3(b) is obtained based on this procedure. We estimate the minimum LOD around peak I as $1.00 \times 10^{-4}$ RIU. On the other hand in Eq. (5), $\left|\frac{\delta \lambda}{\delta n}\right|_I$ and $\left|\frac{\delta I}{\delta \lambda}\right|_I$ are the spectral sensitivity $S_{RI}^\lambda$ shown in Fig. 2(d) and the gradient of the spectral profile shown in Fig. 2(b) at a fixed intensity, respectively. Values of $S_{RI}^\lambda$ and their LOD are calculated and shown in Table. 1. The minimum LOD is $3.19 \times 10^{-4}$ RIU on the left of peak I where the best $S_{RI}^\lambda$ is 486.53 nm RIU$^{-1}$.

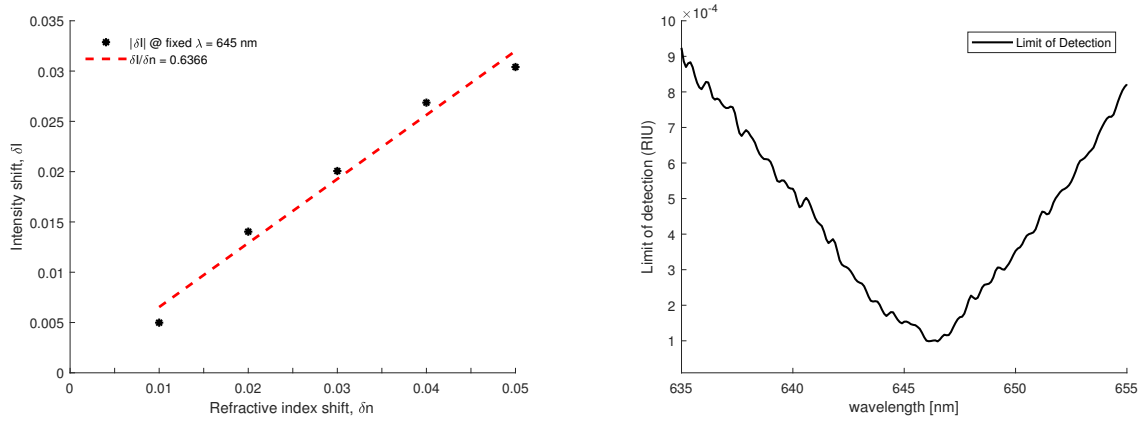


(a) (b)

Figure 3: (a) Refractive index sensitivity based on intensity $S_{RI}^I$ at a fixed wavelength $\lambda = 645$ nm. (b) The calculated LOD as a function of $\lambda$ based on Eq. (4). The LOD at $\lambda = 645$ nm is $1.52 \times 10^{-4}$ RIU and the minimum LOD for the 635 nm - 655 nm band is $1.00 \times 10^{-4}$ RIU.

Table 1: Spectral sensitivity and LOD values calculated using Eq. (5).

| Parameters | Peak I($\lambda_{sp}$) | Peak I(left) | Peak II($\lambda_{sp}$) | Peak II(right) | Peak II(left) |
|---|---|---|---|---|---|
| $S_{RI}^\lambda$ (nm RIU$^{-1}$) | 245.71 | 486.53 | 145.71 | 246.01 | 67.84 |
| LOD (RIU) | $6.30 \times 10^{-4}$ | $3.19 \times 10^{-4}$ | $1.09 \times 10^{-3}$ | $6.71 \times 10^{-4}$ | $2.36 \times 10^{-3}$ |

## 5. Conclusion

We studied an SPR plasmonic sensor based on EOT for the diagnosis of malaria. In this biosensor, the liquid analyte of refractive index ranging from 1.33 (water) to 1.38 (trophozoite stage of malaria infection) is taken to mimic the refractive index of blood cells at different stages of malaria infection. Since the diagnosis technique is based on the principle of variation of a biophysical parameter (refractive index), the shift of maximum transmission peak is monitored, and the spectral sensitivity and LOD thereof are calculated. The transmission resonance peak shifts $\delta\lambda_{sp}$ around the two EOT peaks are linear with the refractive index shifts $\delta n$ of the analyte. The highest spectral sensitivity and LOD of the sensor is 486.53 nm $\text{RIU}^{-1}$ and $3.19 \times 10^{-4}$ RIU on the left of the first peak (635 nm to 655 nm band). On the other hand, based on intensity interrogation, the sensor can attain the minimum LOD of $1.00 \times 10^{-4}$ RIU. The device shows a good sensing performance and thus there is a potential for detecting low percentages of malaria antigens from an infected blood sample. For example, according to Ref. [10], when 10% of red blood cells were infected with plasmodium parasites, the binding of monoclonal antibodies against plasmodium lactate dehydrogenase (a malaria biomarker) produced a 0.004 RIU shift on the sensor surface. The sensor (LOD $\approx 10^{-4}$ RIU) can easily detect this change ($\Delta n = 0.004$) with high resolution.


## Acknowledgments

This project is supported by the African Laser Centre (ALC) grant (ALC-R016) at the South African Council for Scientific and Industrial Research (CSIR). We also acknowledge support from the University of Dar es Salaam, Tanzania, the Laser Research Insitute (LRI) of the University of Stellenbosch, the Department for Science and Innovation (DSI), and the National Research Foundation (NRF) of the Republic of South Africa.


## References


[1] World Health Organization 2021 *World malaria report 2021* (Geneva, World Health Organization)
[2] Fitri L, Widaningrum T , Endharti A, Prabowo M, Winaris N, Nugraha R 2022 *J. Clin. Lab. Anal.* **36** (4)
[3] Bronzan R N, McMorrow M L and Patrick K S 2008 *Mol Diag Ther.* **12** 299–06
[4] Ranadive et al. 2017 *Clin. Inf. Dis.* **64** 1221
[5] Ragavan K, Kumar S, Swaraj S and Neethirajan S 2018 *Biosensors and Bioelectronics* **105** 188-210.
[6] Ankita, Suthar B and Bhargava A 2021 *Plasmonics* **16** 59–63
[7] Rashidnia A, Pakarzadeh H, Hatami, M and Natesan A 2022 *Opt. Quant. Electron* **54** 38.
[8] Briand V, Thilakarathne V, Kasi, R and Kumar C 2012 *Talanta* **99** 113-18
[9] Bhavna S et al. 2014 *Biosensors and bioelectronics* **60** 201-09
[10] Cho S, Briscoe J, Hansen I, Smith J, Chang Y, and Brener I 2014 *IEEE Sensors Journal* **14**(5) 1399-04
[11] Priyamvada J, Babina C, Sanjukta P and Pranab G 2014 *BioMed Research International* **2014**
[12] Vasimalla Y, Himansu S P and Rahul J P 2021 *Heliyon* **7**(3)
[13] Maier S A 2007 *Plasmonics: fundamentals and applications* (Berlin Heideberg: Springer)
[14] Ebbesen T, Lezec H, Ghaemi H, Thio T and Wolff P A 1998 *Nature* **391** 667–69
[15] Bethe H A 1944 *Phys. Rev.* **66** 163–82
[16] Frerik van B, Retif C, Smiet C B, Liu H, Lalanne P and van Exter M P 2012 *Nature* **492** (7429) 411-14
[17] Liu H and Lalanne P 2008 *Nature* **452**(7188) 728-31.
[18] Liu H and Lalanne P 2010 *J. Opt. Soc. Am. A* **27** 2542-50
[19] Popov E, Neviere M, Enoch S and Reinisch R 2000 *Physical Review B.* **62** 16100-08
[20] Martín-Moreno L et al. 2001 *Phys. Rev. Lett.* **86** 1114-17
[21] Zyablovskii A A et al. 2017 *J. Exp. Theor. Phys.* **125** 175-88
[22] Monteiro J P et al. 2013 *Sensors and Actuators B: Chemical* **178** 366-70
[23] Yue W, Wang Z, Yang Y, Li J, Wu Y, Chen L, Ooi B S, Wang X and Zhang X 2014 *Nanoscale* **6**(14) 7917-23
[24] Akpa M A, Konan K, Tokou Z, Kossonou Y, Dion S, Kaduki K and Zoueu J 2019 *Sensors* **19** 3045
[25] Rakić A, A B Djurišić, J Elazar and M L Majewski 1998 *App. Opt.* **37** 5271-83.
[26] Homola J 2008 *Chem. Rev.* **108**(2) 462-93.
[27] Changhyoup L et al. 2021 *Chem. Rev.* **121**(8) 4743–4804